International Journal of ChemTech Research
CODEN(USA): IJCRGG ISSN : 0974-4290
Vol.6, No.1, pp 222-235, Jan-March 2014

Studies on Lithium Sulphanilate Hydrate (LS) single crystal and its Characterization

M. Anantharaja and R. Gopalakrishnan*

Crystal Research Lab, Department of Physics, Anna University, Chennai – 600 025.

***Corres. author. krgkrishnan@annauniv.edu, krgkrishnan@yahoo.com**
Tel: +91-44-2235 8710 / 8707; Fax: +91-44-22358700

Abstract : Lithium Sulphanilate Hydrate (LS) was synthesized and successfully grown as bulk single crystal of size 50 × 10 × 5 mm^3 by the slow evaporation solution growth method using double distilled water as a solvent. The grown crystals were studied for the structural, optical, thermal and mechanical properties. The lattice parameters of the grown crystal are confirmed by single crystal and powder X- ray diffraction methods. The presence of functional groups in the grown crystal was identified from FT-IR and FT Raman measurements. The TG - DTA evaluates the thermal properties of the grown crystal. The transparency of the grown crystal was investigated by recording UV- Vis analysis and optical bandgap of the material was calculated. The dielectric permittivity, dielectric loss and conductivity over a range of frequencies and temperatures have been studied. The Vickers microhardness measurements were carried out on the grown crystals to estimate the mechanical properties. The growth mechanism was identified from the chemical etching studies.
Keywords: A1.Crystal growth; A1. Characterization; A1. Optical properties; B1.Organic compounds; B2.Dielectric properties.

1.Introduction

Materials with nonlinear optical properties have wide applications in modern optical and optoelectronic devices. Organic crystals possess high efficiency of frequency conversion, moderately high damage threshold, wide range of optical transparency [1, 2]. In the recent years, efforts have been made on organic-materials mixed amino acid crystals, in order to improve the chemical stability, laser damage threshold and nonlinear optical properties [3]. Several researchers have carried out a lot of studies on pure and organic, and metal ions-doped crystals [4 - 6].

Sulphanilic acid (SA) (C_6H_4 NH_3^+ SO_3^-) is a promising and interesting compound, which finds a number of applications including nonlinear optics. Sulphanilic acid possesses several good features of good dosimeter and is characterized by its simple spectrum.Sulphanilic acid is nearly tissue equivalent which enables its use in radiation therapy dosimetry, also it is isotropic and its detection limit is about 100 ± 30 mGy. Among many investigated dosimeters, the SO_3^- anion was used by several authors [7, 8] and it has been proved to have quiet consistent dosimetric properties. Sulphanilic acid was already reported to possess dosimetric

properties [9]. The Sulphanilic acid compound displays an anionic part and a cationic part, indicative of the Zwitterionic structure.Sulphanilic acid crystallizes in the orthorhombic structure with space group of P_{bca}[10].

In the present investigation, Lithium Sulphanilate Hydrate (LS) was synthesized by slowly evaporating the solvent. Sulphanilic acid and lithium carbonate in stoichiometric ratio of (1:1) were taken and grown as a single crystal. LS crystallizes in the monoclinic crystal structure with space group $P2_1/c$ and the lattice parameters are a = 5.3430 (10) Å, b = 7.9700 (10) Å,c = 19.490 (3)Å, α = γ = 90°, β = 94.099 (10) ° and V = 827.8(2) $Å^3$.The results on growth and characterization are presented in details.

2. Experimental procedure

2.1. Synthesis and Growth

Lithium Sulphanilate Hydrate (LS) was synthesized from the mixture of commercially available Sulphanilic acid and Lithium carbonate in a stoichiometric ratio of 1:1 at room temperature (35 °C). 17.36 g of Sulphanilic acid were dissolved in 100 ml of distilled water, few of Sulphanilic acid salts arenot dissolved in the solvent due to low solubility in the water. In this mixture 1 mole (7.59 g) of Li_2CO_3 were introduced to the solution. The exothermic reaction takes place, after a period of 1hr continuous string the solutionbecomes clear. The reaction mechanism of LS is presented in the Fig.1.

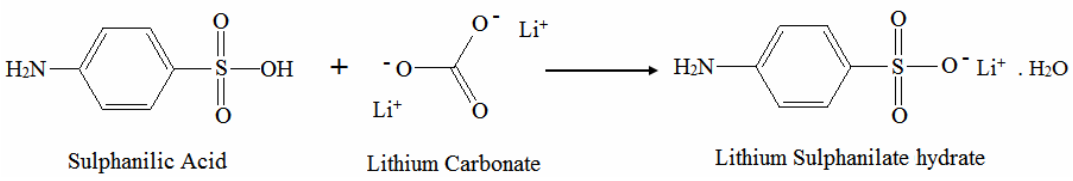

Fig.1. Reaction mechanism of Lithium Sulphanilate Hydrate

The saturated solution of LS was obtained by dissolving the synthesized salt with continuous stirring of the solution using a magnetic stirrer at room temperature (35°C). On reaching saturation, the beaker containing the growth solution was optimally covered and housed in constant temperature bath (±0.01ºC). Good transparent bulk single crystal of LS of size (50 × 10 × 5 mm^3) was harvested from mother solution after 40 days. The grown crystal was found to be stable, non-hygroscopic at ambient temperature as is shown in Fig.2.

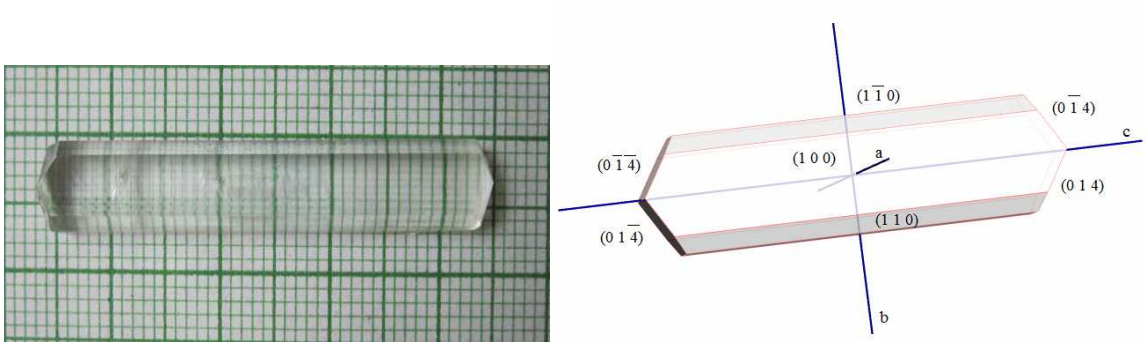

Fig. 2. Grown Crystals and Morphology of Lithium Sulphanilate Hydrate

2.2. Solubility

It is known that the choice of solvent provides some control over crystal habit and this effect depends on the interaction of the surface of the growing crystal. Hence to investigate the crystalline habit of LS in

water, ethanol and DMF were tried. After attaining saturation, the equilibrium concentration was analyzed gravimetrically and the solubility curves were drawn. The solubility increases linearly with temperature in the growth region indicate the title compound possesses positive temperature coefficient is shown in Fig. 3. It was found that the magnitude of solubility was slightly more in water. It was found that the title compound has a positive temperature coefficient.

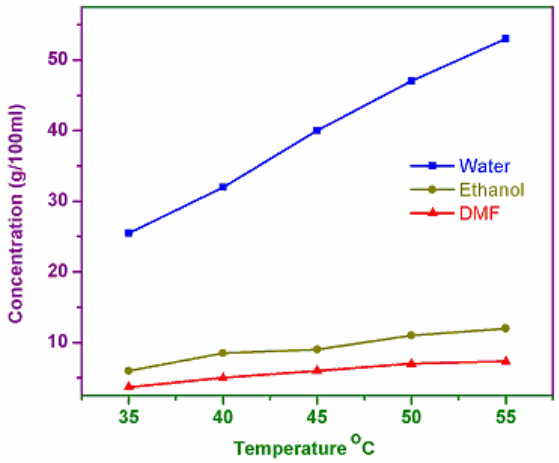

Fig. 3. Lithium Sulphanilate HydrateSolubility curve.

The solubility studies were carried out using water between the ranges of 35°C to 55°C. The solubility was determined by dissolving the recrystallization salt in double distilled water.

3. Characterization studies

The single crystal X-ray diffraction (XRD) analysis was carried out using ENRAF NONIUS CAD4 X-ray diffractometer and its lattice parameters were determined. FTIR spectrum was recorded using BRUKER 66V FTIR spectrometer. The FTIR spectrum of LS was recorded between 4000 – 400 cm^{-1} by the KBr pellet technique. The vibrational frequencies of the grown crystals were verified by FT Raman analysis using BRUKER RFS 27 spectrometer. The thermal behavior was studied by thermogravimetric analysis using a NETZSCH STA 409C/CD thermal analyzer in the nitrogen atmosphereat a heating rate of 10 ºC / min. UV-Visible spectrum was recorded in the region of 280 – 800 nm using VARIAN CARY 5E spectrometer. The dielectric permittivity, dielectric loss and conductivity of the Lithium Sulphanilate Hydrate (LS) were studied using a HIOKI 3532-50 LCR Hitester. The Vickers microhardness test was carried out using a MATSUZAWA microhardness tester with diamond indenter. Chemical etching method was used to identify the dislocation sites and defects in the crystal surface. Etch patterns were observed using an optical microscope (LeitzWetzler) in the reflection mode (400 × M). The details of the results are elaborated in the proceeding sections.

4. Results and discussion

4.1. X-ray crystal structure determination

The unit cell parameters and the crystal structure were determined from single crystal X-ray diffraction data obtained with a three circle Bruker platform diffractometer (graphite monochromated, MoKα = 0.71073A). The unit cell parameters of the LSD crystal were measured at 293 (2) K. The data were integrated using Bruker SAINT; corrections for absorption and decay were applied using Bruker SAINT. The crystal structure was solved by a direct method with the SHELXS – 97 program and refined by the SHELXL 97 program [11] to an R – value of 0.0252. The ORTEP drawing was performed with the ORTEP3 program [12]. The LSD crystal data, experimental conditions and structural refinement parameters are presented in Table1. The crystal structure and packing diagram of LSD are delineated in Figs.4 and 5, respectively, and values of bond lengths and bond angles are listed in Tables 2 and 3. The hydrogen bonds present in the crystal structure are listed in Table 4 and shown in Fig.4.

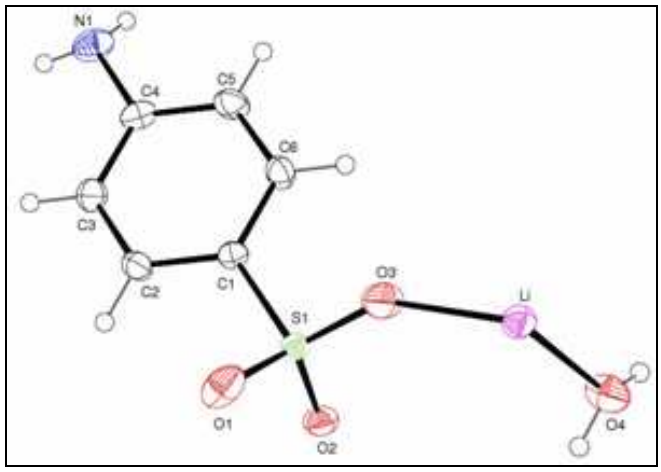

Fig.4. Structure of LSD showing 30% probability ellipsoids and the labeling scheme.

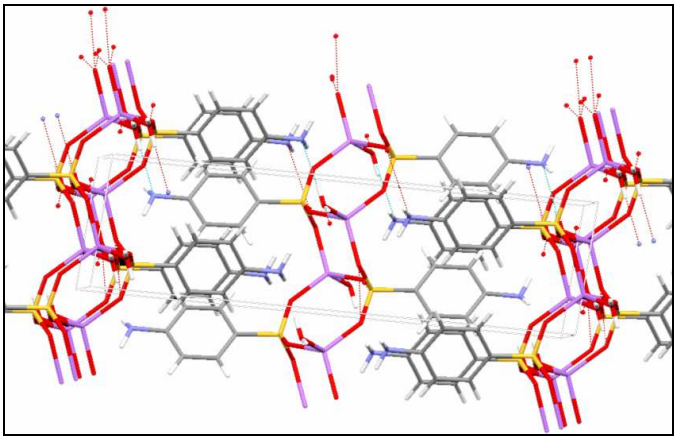

Fig.5. Packing of LSD illustrating the hydrogen bonding scheme.

Table 1. Crystal data and structure refinement for LS

Identification code	Lithium Sulphanilate Dihydrate
Empirical formula	$C_6H_8LiNO_4S$
Formula weight	197.13
Temperature	293(2) K
Wavelength	0.71073 Å
Crystal system, space group	Monoclinic, P21/c
Unit cell dimensions	a = 5.3430(10) Åα = 90°.
	b = 7.9700(10) Åβ = 94.099(10) °.
	c = 19.490(3) Å γ = 90°.
Volume	827.8(2) $Å^3$
Z, Calculated density	4, 1.582 Mg/m^3
Absorption coefficient	0.366 mm^{-1}
F(000)	408
Crystal size	0.30 x 0.20 x 0.20 mm
Theta range for data collection	2.10 to 25.00°.
Limiting indices	-6<=h<=6, -9<=k<=9, -23<=l<=23
Reflections collected / unique	7228 / 1462 [R(int) = 0.0252]
Completeness to theta = 25.00	100.00%
Absorption correction	Semi-empirical from equivalents
Max. and min. transmission	0.9345 and 0.8954
Refinement method	Full-matrix least-squares on F^2
Data / restraints / parameters	1462 / 6 / 135

Goodness-of-fit on F^2	1.11
Final R indices [I>2sigma(I)]	R1 = 0.0272, wR2 = 0.0722
R indices (all data)	R1 = 0.0281, wR2 = 0.0729
Extinction coefficient	0.142(5)

Table 2. Bond lengths (Å) in LS molecule

C(1)-C(6)	1.384(2)	N(1)-H(1B)	0.845(16)
C(1)-C(2)	1.385(2)	O(1)-S(1)	1.4451(13)
C(1)-S(1)	1.7589(16)	O(1)-Li#1	1.932(3)
C(2)-C(3)	1.376(2)	O(2)-S(1)	1.4558(12)
C(2)-H(2)	0.93	O(2)-Li#2	1.939(3)
C(3)-C(4)	1.386(2)	O(3)-S(1)	1.4399(14)
C(3)-H(3)	0.93	O(3)-Li	1.904(3)
C(4)-C(5)	1.384(3)	O(4)-Li	1.945(3)
C(4)-N(1)	1.405(2)	O(4)-H(4B)	0.832(16)
C(5)-C(6)	1.377(2)	O(4)-H(4A)	0.838(16)
C(5)-H(5)	0.93	Li-O(1)#1	1.932(3)
C(6)-H(6)	0.93	Li-O(2)#3	1.939(3)
N(1)-H(1A)	0.853(16)		

Table 3. Bond angles (deg) in LS molecules

C(6)-C(1)-C(2)	119.87(15)	H(1A)-N(1)-H(1B)	111(2)
C(6)-C(1)-S(1)	120.24(12)	S(1)-O(1)-Li#1	142.78(12)
C(2)-C(1)-S(1)	119.79(12)	S(1)-O(2)-Li#2	130.51(11)
C(3)-C(2)-C(1)	120.11(15)	S(1)-O(3)-Li	145.84(12)
C(3)-C(2)-H(2)	119.9	Li-O(4)-H(4B)	131.1(17)
C(1)-C(2)-H(2)	119.9	Li-O(4)-H(4A)	108.1(17)
C(2)-C(3)-C(4)	120.36(16)	H(4B)-O(4)-H(4A)	110(2)
C(2)-C(3)-H(3)	119.8	O(3)-S(1)-O(1)	113.64(10)
C(4)-C(3)-H(3)	119.8	O(3)-S(1)-O(2)	111.49(8)
C(5)-C(4)-C(3)	119.15(15)	O(1)-S(1)-O(2)	111.23(8)
C(5)-C(4)-N(1)	119.80(16)	O(3)-S(1)-C(1)	105.87(8)
C(3)-C(4)-N(1)	120.97(17)	O(1)-S(1)-C(1)	105.99(7)
C(6)-C(5)-C(4)	120.82(16)	O(2)-S(1)-C(1)	108.18(7)
C(6)-C(5)-H(5)	119.6	O(3)-Li-O(1)#1	109.29(15)
C(4)-C(5)-H(5)	119.6	O(3)-Li-O(2)#3	112.94(15)
C(5)-C(6)-C(1)	119.68(16)	O(1)#1-Li-O(2)#3	113.99(15)
C(5)-C(6)-H(6)	120.2	O(3)-Li-O(4)	115.82(16)
C(1)-C(6)-H(6)	120.2	O(1)#1-Li-O(4)	99.64(14)
C(4)-N(1)-H(1A)	112.5(16)	O(2)#3-Li-O(4)	104.53(14)
C(4)-N(1)-H(1B)	113.0(19)	O(2)#3-Li-O(4)	104.53(14)

Table 4. Hydrogen bonds in LS molecule

D-H...A	d(D-H)	d(H...A)	d(D...A)	<(DHA)
N(1)-H(1A)O(4)	0.853(16)	2.408(16)	3.257(3)	174(2)
O(4)-H(4B)O(2)	0.832(16)	2.017(17)	2.8392(19)	170(3)
O(4)-H(4B)S(1)	0.832(16)	2.97(2)	3.7094(15)	150(2)
O(4)-H(4A)N(1)	0.838(16)	2.124(16)	2.929(2)	161(2)

Symmetry transformations used to generate equivalent atoms: #1 -x+2,-y,-z #2 x-1,y,z #3 x+1,y,z #4 x-1,-y+1/2,z+1/2, #5 -x+2,-y+1,-z #6 x,-y+1/2,z-1/2.

4.2. Powder X-ray diffraction analysis

Powder X-ray diffraction patterns were collected using BRUKER D2 PAHSER spectrometer with CuKα (λ = 1.5418Å) radiation by crushing the LS crystals into fine powder. The sample was scanned over the range 10 - 60° at a rate of 1°/min which reveals well defined Bragg's peaks at specific 2θ angle and the crystallographic planes were indexed. The resulting spectrum of LS is as shown in Fig. 6.

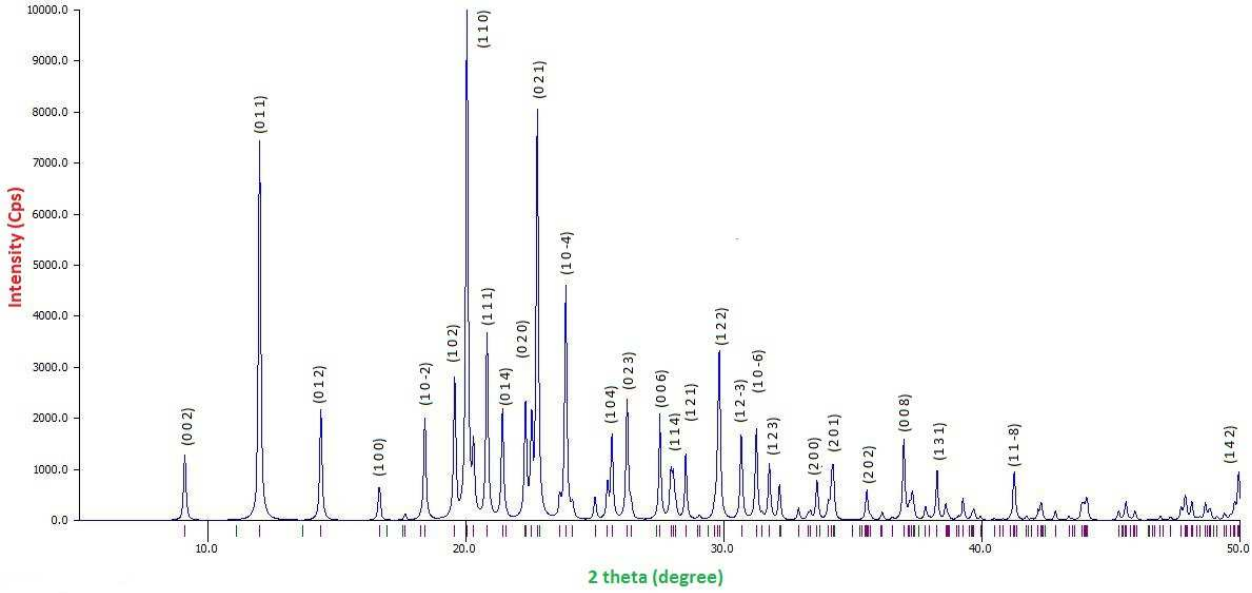

Fig. 6. Powder XRD pattern of Lithium Sulphanilate Hydrate

4.3. Fourier Transform Infrared Analysis

Raman analysis has been a proven technique for the investigation of the molecular structure. The FT-IR analysis of LS was carried out to investigate the presence of functional groups and their vibrational modes. The sample was prepared using KBr pellet technique and the observed spectrum of LS is shown in Fig.7. The vibrational frequencies of title compound LS were identified and their various assignments are listed in Table 5.

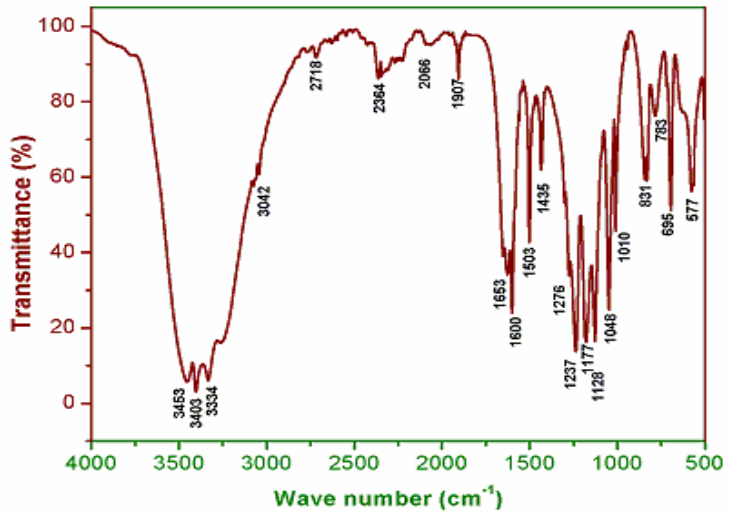

Fig. 7. FTIR spectrum of Lithium Sulphanilate Hydrate

Table 5. Observed IR and Raman bands of LS and their assignments

FT-IR (cm^{-1})	Raman (cm^{-1})	Assignment	Functional group
3453, 3403	-	O-H stretch	Alcohols
3334	-	N-H stretch	1º, 2º amines
3042	3074	=C - H stretch	Alkenes
2718	-	H-C=O stretch	Aldehydes
1653	-	-C=C- stretch	Alkenes
1600	1599	C-C stretch (in ring)	Aromatics
1503	-	N-C asymmetric stretch	nitro compounds
1276	1281	C-N stretch	aromatic amines
1237	-	C-O stretch	carboxylic acids
1177, 1128, 1048 and 1010	1182, 1128 and 1053	C-N stretch	aliphatic amines
831, 783	830	N-H wag	1º, 2º amines
695	700	-C ≡C-H bend	Alkynes
577	584	C-Br stretch	alkyl halides

4.4. FT Raman Analysis

The FT Raman spectrum was recorded in region 4000 – 500 cm^{-1} in stokes region using the 1064 nm line of an Nd:YAG laser excitation with 100mW power. The resulting FT Raman spectrum is shown in Fig.8. The vibrational frequencies of Lithium Sulphanilate Hydrate were identified and their assignments are listed in Table 5. From the table it is inferred that LS protonates the carboxyl group.

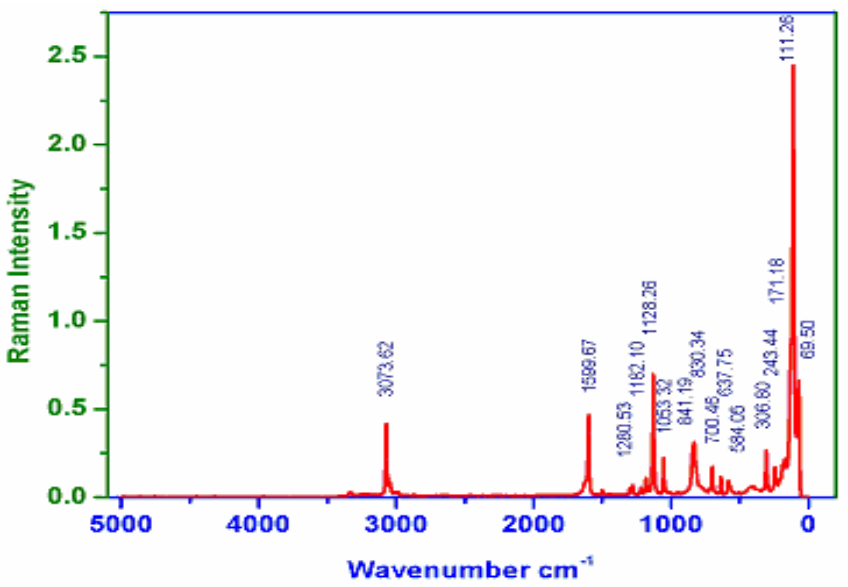

Fig.8. FT Raman spectrum of Lithium Sulphanilate Hydrate

4.5. Thermal analysis

Thermograms provide information about decomposition patterns of materials and weight loss also[13]. The thermogravimetric analysis (TGA) of Lithium Sulphanilate Hydrate was carried out between 80 - 800 ºC in nitrogen atmosphere at a heating rate of 10 ºC / min (Model: NETZSCH STA 409). There is no weight loss up to 140 ºC, which clearly illustrates the absence of physical adsorption. A single intense weight loss starts at about 165 ºC and it is assigned to the water molecules ofLS. The title material has started to decompose at 318 ºC. Based on this observation it can be said that the compound is completely volatilized up to 499 ºC. The resulting LS thermal spectrum is as shown in Fig. 9.

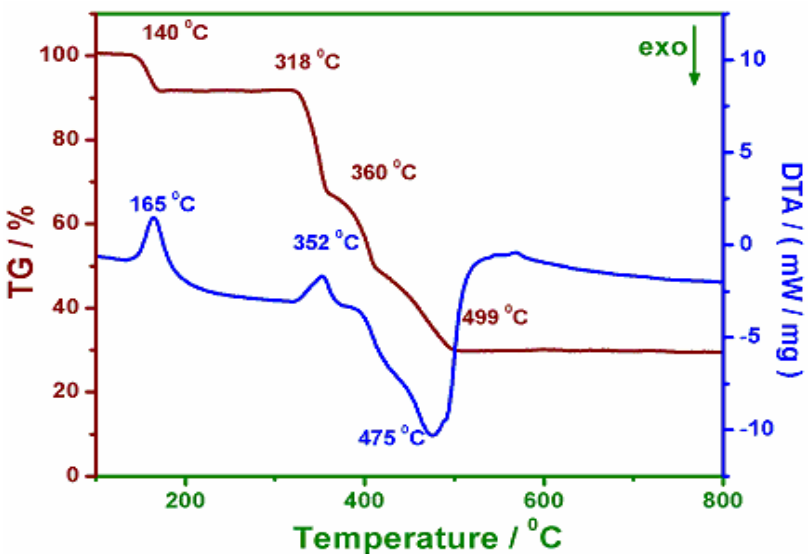

Fig. 9. Trace of Thermal analysis of LS

In the trace of Differential Thermal Analysis (DTA), there is a sharp endothermic peak at about 352 ºC, which is assigned to melting point of the grown crystal. This is followed by a broad exothermic peak at 475 ºC shows that LSstarts to decompose. In the DTA trace no other endothermic or exothermic peaks are observed which suggest the absence of any isomorphic transformation below its melting. The sharpness of the endothermic peak shows good degree of crystallinity of the grown ingot.

4.6. UV- visible studies

UV-vis-NIR spectral study may be assisted in understanding the electronic structure of the optical band gap of the crystal. The study of the absorption edge is essential in connection with the theory of electronic structure, which leads to the prediction of whether the band structure is affected near the band extreme. The grown LS crystals were cut and polished of thickness 2mm was subjected to absorption measurements in the spectral region 280 - 800 nm. The recorded spectrum as is shown in the Fig. 10 (a and b).

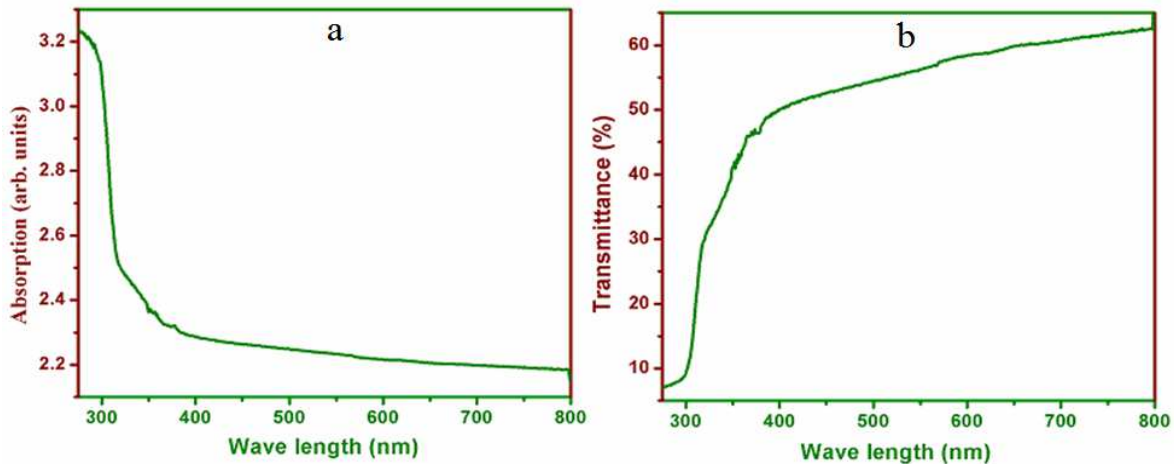

Fig. 10. (a). UV-vis-NIR absorption spectrum of LS crystal
(b). UV-vis-NIR transmittance spectrum of LS crystal

A sharp fall in the transmittance at 310 nm corresponds to the fundamental absorption (UV cut-off wavelength) of the title compound. Absorption in the near- ultra violet region arises from electronic transitions associated within the samples.The absence of absorption of light in the visible region is an intrinsic property of all amino acids [14].From the transmittance spectra, it is noticed that LScrystal has high transmittance in the entire visible–NIR region of the spectra and this property enables the materials for optoelectronic applications.

4.7. Optical band gap

The optical absorption coefficient (α) of LScrystal at different wavelength was calculated using the relation,

$$\alpha = \frac{2.3026 \log(1/T)}{d} \quad (1)$$

where T is the transmittance and d is the thickness of the crystal. As an indirect band gap material, the crystal has an absorption coefficient (α) obeying the following relation for high photon energies (hv)

$$\alpha = A \frac{(h\upsilon - E_g)^{1/2}}{h\upsilon} \quad (2)$$

whereEg is the optical band gap of the crystal and A is a constant. Optical band gap calculated from the UV-Vis absorbance data (Fig.11).

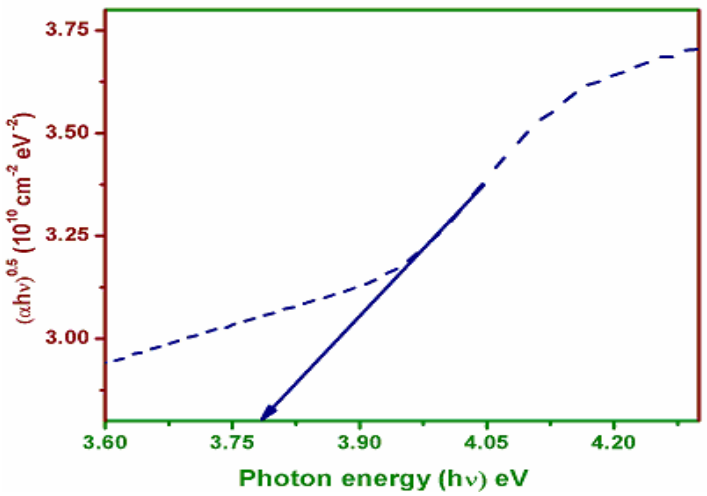

Fig. 11. Optical band gap of LScrystal

The plot between Energy (hυ) and $(\alpha h\upsilon)^{1/2}$ is made (where α is the absorption coefficient) and the optical band gap energy is found to be 3.83eV by extrapolating the slope region (where it cuts the X-axis) [15].

4.8. Dielectric studies

The dielectric parameters depend on the frequency of the ac voltage applied across the material. The sample was cut and polished using wet cloth polishing sheet. The sample dimensions were 18 mm × 3 mm surface area and 4 mm thickness. Silver paste electrodes on opposite sides ensure good electrical contacts. The dielectric measurements were carried out in the frequency range 50 Hz – 5 MHz at temperatures 40, 60 and 80 ^{0}C. The variation of dielectric permittivity (ε_r), dielectric loss and conductivity with frequency also shows a similar trend for other organic materials [16]. The dielectric permittivity and dielectric loss increase with increase in temperature. The dielectric constant of a material is generally composed of four types of contributions, viz. ionic, electronic, orientational and space charge polarization [17].

All polarizations are active at low frequency. The nature of variations of dielectric permittivity with frequency and temperature indicates the type of contributions that are present in them. The large value of dielectric permittivity at low frequency is due to the presence of space charge polarization, which depends on the purity and perfection of the sample (Fig.12(a)). In normal dielectric behavior, the dielectric constant decreases with increasing frequency and reach a constant value, depending on the fact that beyond a certain frequency of the electric field, the dipole does not follow the alternating field with increasing frequency, the dielectric loss and dielectric permittivity values decrease which depend on the excitation of bound electrons, lattice vibrations. Therefore the polarization decreases and exhibits reduction in the value of ε_r[18].

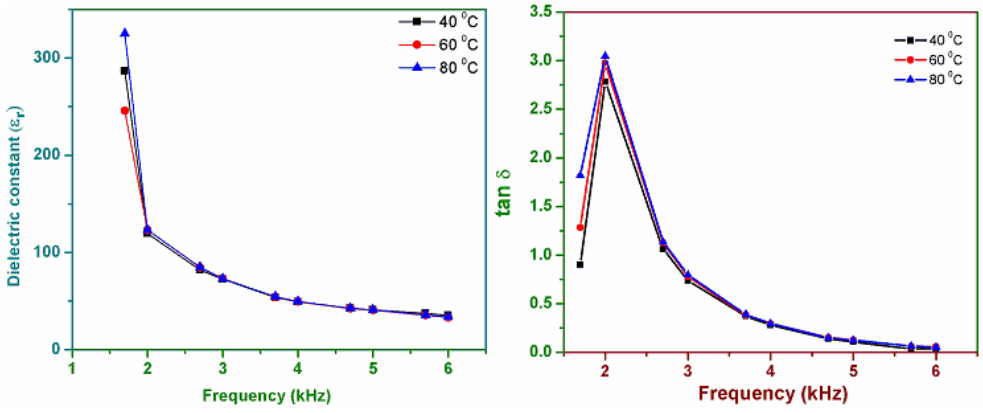

Fig. 12a) Dielectric tensor vs. log f b)tan δ vs. log f

The dielectric loss is also studied as a function of frequency at different temperatures (Fig. 12 (b)).

These results suggest that the dielectric loss strongly depends on the frequency of the applied field, similar to what commonly happens with the dielectric behavior in the ionic system. As a result there is a rise in conductivity at higher temperature (Fig.12 (c)) [19]. The variations of dielectric permittivity ε_r with temperature and frequency are shown in Fig.12 (d) which indicates the temperature independent property of ε_r, owing to immobilization of local charge carriers. The dielectric permittivity (ε_r) of a crystal is expressed by a second order tensor [20]. Generally the low value of dielectric loss indicates that sample possesses good crystalline quality with fewer defects.

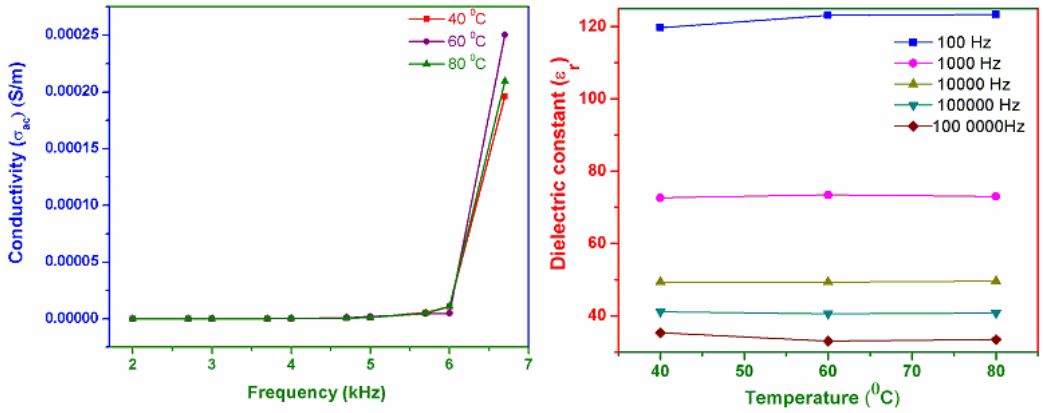

Fig. 12 a) Conductivity vs. log f b)Dielectric permittivity vs. temperature

4.9. Vickers microhardness measurement

Hardness of the material is a measure of the resistance it offers for local deformation. It plays a key role in device fabrication [21]. The structure and compositions of the crystalline solids are inviolably related to the mechanical hardness. Microhardness testing is one of the best methods of understanding the mechanical properties of materials such as fracture behavior, yield strength, brittleness index and temperature of cracking [22-23].

Vickers hardness studies were carried out at room temperature on the grown LS crystal to investigate its mechanical strength. The indentation time was kept as 5 sec for all the loads varying from 1 to 100 g. Three trials were made for each load and the average diagonal length of the indentation marks was calculated and the microhardness values were calculated using the relation-

$$H_v = 1.8544 \frac{P}{d^2} kg / mm^2$$

whereH_v is the hardness number and P is the load applied in gram and d the diagonal length of the impression in micrometer. Cracks at the corners of the indentation diagonal were observed for higher loads. The crack length was measured from the center of the indentation mark up to the tip of the crack. The fracture toughness Kc for c/a >2.5, where c is the crack length and a is the half diagonal length of the indentation mark, is calculated using relation [24].

$$K_c = \frac{kP}{c^{3/2}}$$

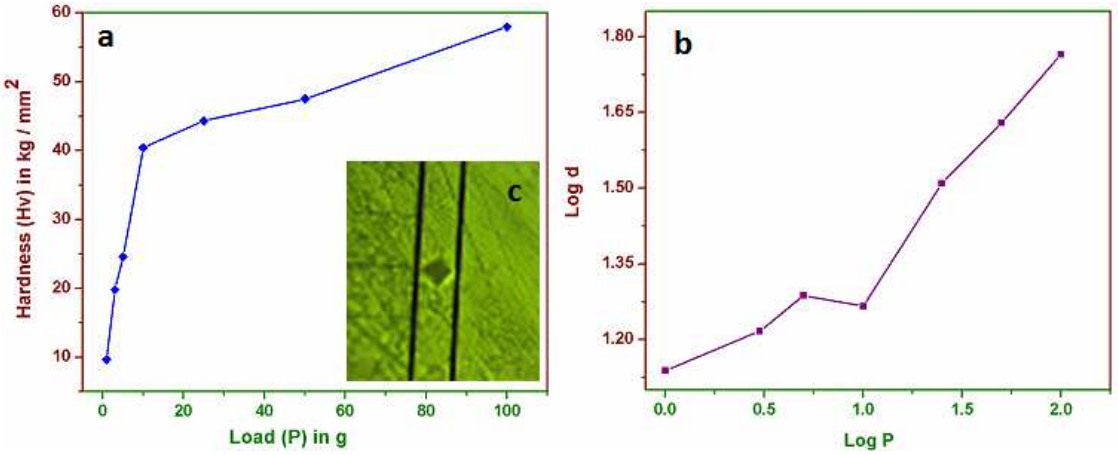

Fig.12(a) Microhardness number (H_V) vs. load (*P*) (b)Log P vs. Log d of LS single crystal (c) Indentation impression

where the constant **k = 1/7** for the Vickers indenter. From fig. 12(a) it is observed that hardness value increases with increase of load, hence the material exhibits reverse indentation size effect.

It is found that LS crystals can withstand loads up to 25 g above which the cracks are developed and 100 g the crystal completely breaks. However, with the increase in the depth of penetration, the defect of inner layers become more and more prominent and ultimately the value of $H_v$decreases. The fracture toughness Kc determines quantity of fracture stress applied under uniform loading for a crystal with well-defined cracks, wherein the resistance to fracture indicates the toughness of a material. In the present case the cracks appear for c/a < 2.5 and P ≥ 25g. The fracture toughness Kc is 0.01236.

4.1. Etching

The crystals with defects may destroy the mechanical, optical and electrical properties, which affect the usefulness of the crystals. The chemical etching studies were carried out on the grown single crystals of LS to study the symmetry of the crystal face from the shape of etch pits, and the distribution of structural defects in the grown crystals [25].

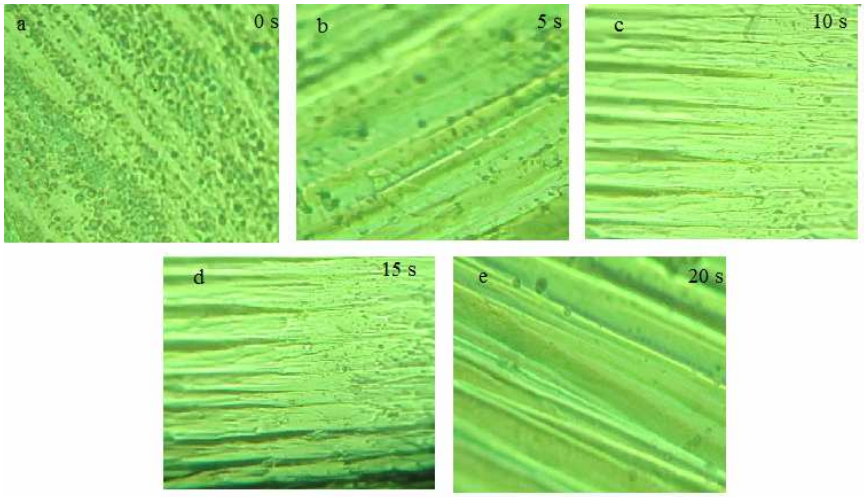

Fig. 12: Etch pit patterns of LS single crystal (a) Before etching, (b) 5 s, (c) 10s, (d) 15s, and (e) 20s.

Initially, sample was dipped with the help of water then it was cleaned using a soft tissue paper.

Different etch patterns were observed in Fig 12 (a-e). In the present case, water is used as an etchant at room temperature because water is a superior etchant for revealing the dislocation etch pits and it is insensitive to surface orientation as it produced pits almost on all surface [26]. Fig.12(a) represents as grown crystal surface before etching. Fig.12(b) shows the straight striations. The shape of the etch pit indicates the direction of the dislocation lines. Fig.12(c-e)shows a kinks and parallel layers observed at 20s. These may be due to change in the diffusion field around a dislocation site with increasing etch time.

5. Summary and Conclusion

Good quality single crystal of LS was grown from aqueous solution by slow evaporation solution growth method at room temperature. Single crystal X-ray diffraction analysis reveals that the crystal belongs to the monoclinic structure with space group $P2_1/c$. The cell parameter was confirmed. The FT IR and FT Raman spectroscopic analysis confirmed the functional groups and molecular structure of the compound. The TGA and DTA analysis shows that the crystal is stable up to 318 ºC. The optical absorption study reveals transparency of the crystal with a UV cut-off of 320 nm. The band gap energy for the grown crystal was found to be 3.83 eV. The dielectric studies reveal the low value of dielectric loss indicates that sample possesses good crystalline quality with fewer defects. The microhardness study reveals the mechanical strength of the crystal. Well defined kinks and parallel layers etch pits were observed on grown crystal, the shape of the etch pit indicates the direction of the dislocation lines. Thus, the optical properties, hardness value, and encouraging dielectric properties of the LS crystal indicate the high suitability for optoelectronic applications.

References

1. A.Abdel- Kader, J. Mater. Sci. Mater. Electron., 2 (1991) 7–10.
2. N.Peeresy, M.Souhassouyx, B.Wynckey, G.Avoilleyx, A.Coussonzand, J. Phys. Condens. Matter. 9 (1997) 6555–6562.
3. R.Reintjes, E.C.Eckardt, Appl. Phys. Lett., 30 (1977) 91–93.
4. P.Kumaresan, S.MoorthyBabu, P.M.Anbarasan, Opt. Mater. 30 (2008) 1361–1368.
5. A.P.Voronov, Yu.T.Vyday, V.I.Salo, V.M.Puzikov, S.I.Bonderenko, Radiat. Measurem.,42 (2007) 553 – 556.
6. A.Jayarama, S.M.Darmaprakash, Appl. Surf. Sci., 253 (2006) 944 –949.
7. P. N. Kizer, J. R. Morton, and K. F. Preston, J. Chem. Soc. Faraday Trans., 87 (1991) 3147–3149.
8. J. Morton, F. Ahlers, and C. Schneider, Appl. Radiat. Isotopes. 40 (1993) 851-857.
9. A. Maghraby and E. Tarek, Radiat. Measurem., 41 (2006) 170–176.
10. John N. Low and Christopher Glidewell, ActaCryst. C., 58 (2002) 209–211.
11. S.Haussühl, Zeitschriftfürkristallographie. 212 (1997) 186–190.
12. C.M. Earnet, Anal. Chem., 56 (1984) 1471A–1486A.
13. V. Krishnakumar, R. Nagalakshmi, SpectrochimicaActa Part A Molecular Biomolecular Spectroscopy. 61 (3) (2005) 499–509.
14. K. Ambujam, S. Selvakumar, D. PremAnand, G. Mohamed, P. Sahayaraj, Cryst. Res. Technol. 41 (2006) 671–677.
15. A.Ashour, N.El-kadry, S.A.Mahmoud, Thin Solid Films. 269 (1995) 117–120
16. K.V. Rao, A. Smakula, Journal of Applied Physics. 36 (1965) 2031–2038.
17. P.Suryanarayana, H.N. Acharya, K. Rao, J. Mater. Sci. Lett., 3 (1984) 21–24.
18. K.B.R. Varma, K.V. Ramanaiah, K.V. Rao, Bulletin of Material Science. 5 (1983) 39–48.
19. C. Balarew, R. Duhlew, Journal of Solid State Chemistry. 55 (1984) 1–6.
20. Don Berlincourt, W.R. Cook Jr., Mary Ellen Rander, ActaCryst., 16 (1963) 163–165.

21. Mott, B., Ed. Micro Indenation Hardness Testing; Butterworth: London, 1956.
22. B. R. Lawn and E. R. Fuller, J. Mater. Sci., 10 (1975) 2016–2024.
23. Westbrook, J. H. Report 58-RL-2033 of the G. E. Research laboratory, USA, 1958
24. C. B. Ponton and R. D. Rawlings, Br. Ceram. Trans. J., 88 (1989) 83–90.
25. K. Sangwal (Ed.), Etching of Crystals, North-Holland Physics Publishing, the Netherlands, 1987.
26. S. Mukerji, T. Kar, J. Cryst. Growth. 200 (1999) 543–549.

*****